JOURNAL OF GUIDANCE, CONTROL, AND DYNAMICS
Vol. 15, No. 2, March-April 1992

High-Alpha Application of Variable-Gain Output Feedback Control

Aaron J. Ostroff*
NASA Langley Research Center, Hampton, Virginia 23665

This paper describes a recently developed variable-gain, optimal, discrete, output feedback design approach that is applied in a nonlinear flight regime. The flight regime covers a wide angle-of-attack α range that includes the stall region. The paper contains brief descriptions of the variable-gain formulation, the discrete-control structure and flight equations used to apply the design approach, and the high-performance airplane model used in the application. Both linear and nonlinear analyses are shown for a longitudinal four-model integrated design case with $\alpha = 5$, 15, 35, and 60 deg and two flight control modes. Nonlinear simulations show good time response for both a longitudinal pitch-up and pitch-down maneuver and α regulation within 5 deg from the nominal angle during a high-α lateral maneuver.

Introduction

HIGH angle-of-attack α flight is a desirable capability because of potentially large payoffs for combat aircraft. These airplanes will have to operate over a wide flight regime that includes stall and poststall, creating the need for controlled flight far beyond the maximum aerodynamic lift angle of attack. One goal is to make airplanes pitch up and roll faster at high α, which drives up the pitch and yaw control power requirements. The problem is that the control power of conventional airplanes decreases as airspeed decreases. Research is under way on methods to improve controllability at high α where control power is low and departures are most likely. One solution to the control power problem is the use of thrust vectoring controls that provide additional control power for stability augmentation as well as for maneuver enhancement in the stall and poststall flight regimes.

The requirement for airplanes to operate with agility over a highly nonlinear flight regime puts additional burden on control law designers. A linear single-point design with constant feedback gains is probably inadequate to maintain good control properties over the complete α range. Typically, control designers develop satisfactory control laws at several points over the flight regime and then use an interpolation technique, straight line approximation or a least squares fit, to obtain final control gains. When more than one independent variable is involved, gains determined from several best fit curves often get multiplied. One potential problem with this approach is that the controller may lose performance characteristics and even stability in high-order, highly sensitive plants.

An objective of this research is to extend the operating range of the control law over the flight regime while continuing to use established linear control design and analysis techniques. In other words, the objective is to design a nonlinear feedback control law using linear theory. The control methodology is an extension of previous developments for a direct-digital feedback design.[1] This paper describes the application to high-α flight of a variable-gain optimal output feedback control design methodology[2-4] in which the feedback gains are calculated and scheduled as a function of one design parameter α. In general, several variable-gain design parameters, either linear or nonlinear, may be used. Desired control characteristics are specified by selecting optimal weightings and variable-gain design parameters prior to designing the controller, negating the need for interpolation or gain-fitting techniques. Each of the operating points considered in the design has a local quadratic cost function and is guaranteed to be stable at the design point. A global cost, which is the weighted sum of the various local costs, is minimized within the algorithm. The variable-gain methodology is relatively new, and the research described in this paper is one of the first applications.

The variable-gain formulation is discussed in the first section of this paper and is followed by a description of a discrete control law structure that has been used successfully in other direct-digital design applications.[5-8] The third section includes a brief description of the airplane model used for this application. The section on the design example includes a description of four longitudinal linear design models and their associated linear analysis. The final section considers the nonlinear simulation and includes some practical aspects that must be considered, as well as variable-gain scheduling results. Two different maneuvers are shown for the variable-gain scheduling example.

Variable-Gain Formulation

Variable-gain output feedback is an outgrowth of a stochastic, optimal, discrete, output feedback design approach for single-point control designs.[1] Typically, single-point designs are combined by using a curve fitting approach, such as a linear approximation or a higher-order least-squares fit. In contrast, the variable-gain approach[2-4] solves an integrated control design problem by simultaneously incorporating characteristics for an ensemble of systems. In the equations that follow, all variables are shown to be a function of the argument p, which in the general case represents various parameters that define each system operating point.

A standard quadratic function $\bar{J}[p,K(p)]$ is used to describe the discrete local cost at each operating point and has the form

$$\bar{J}[p,K(p)] = \lim_{N\to\infty} \frac{1}{2(N+1)} \sum_{k=0}^{N} E[X(p,k+1)^T \times Q(p)X(p,k+1) + U(p,k)^T R(p)U(p,k)] \quad (1)$$

where $K(p)$ is the feedback gain matrix, $Q(p) \geq 0$, $R(p) \geq 0$, E is the expectation operator, and $X(p)$ and $U(p)$ (to be described later) are augmented state and control vectors, re-

Presented as Paper 89-3576 at the AIAA Guidance, Navigation, and Control Conference, Boston, MA, Aug. 14-16, 1989; received March 9, 1990; revision received Jan. 10, 1991; accepted for publication Feb. 11, 1991.

*Senior Research Engineer, Aircraft Guidance and Control Branch, Guidance and Control Division, Mail Stop 489.

spectively. For simplicity, the cross term between the state and control vectors is not included, although the term is included in the design algorithm. The main objective is to minimize a global cost $J(K)$ expressed by

$$J(K) = \sum_{j=1}^{M} f_j \bar{J}_j[p,K(p)], \qquad f_j \geq 0 \tag{2}$$

where each of the local costs are summed and weighted, $f_j \geq 0$, to assign relative priorities to the M individual operating points. From Eqs. (1) and (2), it is clear that local control laws are neither designed nor optimized, whereas a global controller that considers all operating points is designed without the use of curve fitting techniques.

The discrete stochastic system and measurement equations have the form

$$x(p,k+1) = \Phi(p)x(p,k) + \Gamma(p)u(p,k) + w(p,k) \tag{3}$$

$$y(p,k) = C(p)x(p,k) + \eta(p,k) \tag{4}$$

where $\Phi(p)$, $\Gamma(p)$, and $C(p)$ represent the system matrices; $x(p,k)$, $y(p,k)$, and $u(p,k)$ are the state, measurement, and control vectors, respectively; $w(p,k)$ and $\eta(p,k)$ represent state process noise and sensor noise vectors, respectively; and k is the sampling step. It is assumed that $w(p,k)$ and $\eta(p,k)$ are uncorrelated, zero-mean, white-noise vectors as

$$E[w(k,p)] = 0, \qquad E[\eta(k,p)] = 0 \tag{5}$$

$$E[w(k,p)\eta^T(k,p)] = 0 \tag{6}$$

$$E[w(k,p)w^T(j,p)] = W(p)\delta_{k-j} \tag{7}$$

$$E[\eta(k,p)\eta^T(j,p)] = V(p)\delta_{k-j} \tag{8}$$

where $W(p)$ and $V(p)$ represent process-noise and sensor-noise covariance matrices and δ_{k-j} is the Kronecker delta. Rate control commands $v(p,k)$ are used in the control application, as described in the following section. The rate control command and measurement vectors are related by the feedback gains as

$$v(p,k) = -K(p)y(p,k) \tag{9}$$

which is the standard output feedback form except for dependence on the operating point p.

The form chosen for the feedback gain matrix has a linear functional relationship with the operating point parameters[2] and contains both a constant-gain feedback part, which is the standard case, and a variable-gain feedback part. The variable-gain is implemented by

$$K(p) = K_0 + \sum_{i=1}^{q} p_i K_i \tag{10}$$

It is not feasible to compute the gain $K(p)$ for every possible variable (α, β, etc.) over an entire flight regime, and so a selected set of p_i is used for the variable feedback-gain schedule. This selected set of parameters will be referred to as the variable-gain scheduled parameters in the remainder of this paper. Each of the p_i can be either linear or nonlinear (e.g., v^2), even though Eq. (10) shows a linear functional relationship between feedback gain and the gain-scheduled parameters. In the example design problem described in this paper, one gain-scheduled parameter ($q = 1$) that is a linear function of angle-of-attack α is used.

Internal to the design algorithm, a substitution is made where the p_i is imbedded within the output equations rather than the feedback gains. Redefining Eqs. (4) and (9) as

$$\bar{y}(p,k) = \bar{C}(p)x(p,k) + \bar{\eta}(p,k) \tag{11}$$

$$v(p,k) = -\bar{K}(p)\bar{y}(p,k) \tag{12}$$

where $\bar{C}(p)$ and $\bar{\eta}(p,k)$ are defined in terms of the Kronecker product $\otimes$[9] as

$$\bar{C}(p) = \bar{p} \otimes C(p) \tag{13}$$

$$\bar{\eta}(p,k) = \bar{p} \otimes \eta(p,k) \tag{14}$$

$$\bar{p} = [1 \; p_1 \; \ldots \; p_q]^T \tag{15}$$

$$\bar{K} = [K_0 \; K_1 \; \ldots \; K_q] \tag{16}$$

The feedback gain matrix in Eq. (16) is thus calculated as one large fixed gain matrix with a column dimension corresponding to the row dimension of the augmented output vector [Eq. (11)]. It is beyond the scope of this paper to describe the variable-gain design algorithm, which can be found in Refs. 2 and 3. In general, each operating point is solved iteratively for necessary conditions that include the solution of two Lyapunov equations and a gradient equation. After combining the equations for all operating conditions into a global gradient expression, the feedback gain matrix is then calculated. This feedback gain matrix is accepted only if all operating conditions remain stable and the global cost is reduced. The main point of this variable-gain formulation is to find a variable feedback gain matrix $K(p)$ that minimizes the global cost [Eq. (2)] subject to the constraints defined in Eqs. (3-10).

Control Law Structure

The variable-gain formulation is very general and can apply to a wide range of control structures, but for the application described in this paper, a proportional-integral-filter (PIF) discrete controller structure is selected.[8,10] PIF is a direct digital integrated formulation using linear dynamics for design. The PIF equations and weightings for the local cost function are formulated in the continuous domain and then transformed to the discrete domain. The discrete plant dynamics in Eq. (3) are augmented by additional dynamic equations for control rate and integrators as

$$u(p,k+1) = u(p,k) + (\Delta T)v(p,k) \tag{17}$$

$$z(p,k+1) = z(p,k) + (\Delta T)H_{zy}y(p,k) + (\Delta T)D_z u(p,k) \tag{18}$$

where H_{zy} and D_z are transmission matrices for the states and/or controls to be integrated, $y(p,k)$ is defined in Eq. (4), $z(p,k)$ is the integrator state, $v(p,k)$ is the control rate command described in Eq. (9) and used in Eq. (1) as $U(p,k)$, and ΔT is the discrete sampling period. The new augmented state vector $X(p,k)$ and output vector $Y(p,k)$ are defined as

$$X(p,k) = [x(p,k)^T, u(p,k)^T, z(p,k)^T]^T \tag{19}$$

$$Y(p,k) = [y(p,k)^T, u(p,k)^T, z(p,k)^T]^T \tag{20}$$

The state vector $X(p,k)$ is then used in the local cost equation (1).

The PIF control structure is shown schematically in Fig. 1. The variable feedback gain matrix $K(p)$ is partitioned into

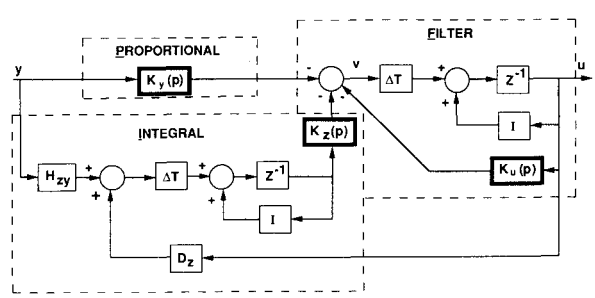

Fig. 1 PIF control structure.

submatrices corresponding to the plant outputs, control position outputs, and integrator outputs, respectively, at any operating point as

$$K(p) = [K_y \; K_u \; K_z] \tag{21}$$

where the outputs of the feedback gain matrices all contribute to v. The time step from rate to control position command u accommodates necessary computation delays. In addition, proportional feedback of u allows additional filtering within each control channel. Only measurable states are fed back and selected outputs are integrated to give type-1 control properties.

All equations are implemented in incremental form using total measurable quantities. This implementation has worked very well with nonlinear dynamics in other applications.[5-7] A significant advantage of this incremental implementation is that trim tables are not required and the airplane automatically goes to a new equilibrium state as the integrated output follows the command.

The main incremental flight control equations[8] are

$$v_k = T_u v_{k-1} + K_y(y_k - y_{k-1}) + T_i(y_{z,k-1} - y_{m,k-1}) + T_f(u_{m,k+1} - u_{m,k}) \tag{22}$$

$$u_{k+1} = u_k + (\Delta T)v_k \tag{23}$$

where y_z is the vector of integrated outputs, y_m the output vector from the command model, u_m the input vector to the command model, and u_k the control position command vector to the plant servoactuators. Using Eq. (21), T_u and T_i become

$$T_u = I - (\Delta T)K_u \tag{24}$$

$$T_i = -(\Delta T)K_z \tag{25}$$

T_f is a matrix composed of feed-forward gains and is not part of the variable-gain formulation. The feed-forward gains are computed by inverting the open-loop plant with the integrator states defined as the outputs. A more complete description is presented in Ref. 11 and Chap. 4.10 of Ref. 10. Since T_f is not part of the variable-gain formulation, straight-line interpolation of these gains was used during nonlinear simulation. A command generator in the feed-forward path could be used to incorporate flying qualities requirements, but this has not been done for the present application; rather, selected design goals were chosen to be generally consistent with good flying quality requirements.

Airplane Model

The model used for this work has the characteristics of a high-performance, high-angle-of-attack airplane that can undertake fighter or attack missions. For this study, the airplane has a gross weight of approximately 33,000 lb, a wing span including tip missiles of 40 ft, and a length of 56 ft. Controls include two afterburner engines plus the following control surfaces: 1) horizontal stabilators, 2) full-span leading-edge flaps, 3) trailing-edge flaps, 4) ailerons, and 5) twin vertical stabilizers. In addition, pitch and yaw thrust vectoring controls have been added for both longitudinal and lateral-directional maneuvering.

Table 1 shows the short period eigenvalues and trim Mach numbers for an α range from 5 to 60 deg at 15,000 ft. The airplane is trimmed straight and level for α up to 35 deg. For α greater than 35 deg, the flight-path angle becomes negative because insufficient thrust is available to maintain level flight. These data in Table 1 show that the short period open-loop eigenvalue becomes very lightly damped when α exceeds 40 deg (poststall flight regime) with the airplane being unstable for α at 50 and 55 deg. The phugoid (not shown) becomes more heavily damped as α increases. Reference 12 contains detailed plots of the aerodynamic force and moment coefficients for this airplane.

The example application described in this paper includes the horizontal stabilator and thrust vectoring controls. The linear design assumes fourth-order dynamics for the stabilator (poles at $-14.9 \pm j33$ and $-62 \pm j85$) and first-order dynamics for the thrust vectoring control (pole at -30).

Design Example

Linear Design Model

An integrated design consisting of four flight conditions (α = 5, 15, 35, and 60 deg) is used for the variable-gain output feedback application. The control law at these four flight conditions includes two command modes to demonstrate task-tailored capability with a transition region between these modes. The four flight conditions include a low-α operating point (5 deg), an operating point at approximately maximum lift (35 deg), a high-α operating point (60 deg), which is the highest α case in an existing linear data base, and a transitions point (15 deg). Additional flight conditions could be used to increase the resolution of the gain schedule, but these four points are sufficient to demonstrate the variable-gain approach. A pitch rate, q-command, mode is used at low α, whereas an α-command mode is used when α is 35 deg or higher with a transition region occurring between these modes. The α command is phased in between 5 and 15 deg of α and the q-comand is phased out between 15 and 35 deg of α. This transition range may not be the optimum choice, but the example does demonstrate a practical capability to incorporate multimode design.

The airplane model used in the design example is discussed in the previous section. The plant has fourth-order longitudinal dynamics for the short period and phugoid modes, two controls (actuator dynamics with five states as described in the previous section) for the horizontal stabilator δ_s, and symmetric thrust vectoring δ_v, as well as three outputs for q, α, and n_z (normal acceleration). The n_z measurement is transmitted through a low-pass filter of 50 rad/s, giving a total of 10 states for the design plant. The advantage of using an output feedback design algorithm is that higher order dynamic models can be included for maximum accuracy. This includes actuator and sensor dynamics and a phugoid mode (stable for the four selected operating conditions), which is not directly modified by feedback in the present application. Since the design algorithm requires a stable closed loop, an unstable phugoid mode would require either a stable approximation or truncation of the phugoid mode; in this latter case, the designer would use a short-period approximation for the plant model.

The PIF controller used in this example has six states. Two of the states are created by feeding back the control position commands [Eq. (17)], which generates additional low-pass filtering. Two additional states are created by adding integrators (18) to either q or α (depending on the mode) and to δ_v. The α integrator provides a type-1 system with zero steady-state error to the commanded variable, the q integrator provides a type-0 system since the plant transfer function from

Table 1 Short period open loop

		Eigenvalue	
α	Mach	Real	Imaginary
5	0.46	−0.55	1.30
10	0.33	−0.37	0.66
15	0.28	−0.28	0.87
20	0.26	−0.25	0.64
25	0.24	−0.25	0.36
30	0.22	−0.24	0.58
35	0.20	−0.27	0.56
40	0.19	−0.27	0.69
45	0.19	−0.033	0.73
50	0.19	0.019	0.83
55	0.19	0.023	1.17
60	0.20	−0.017	1.07

control input to q has a zero in the numerator that counteracts the controller integrator pole, and the δ_v integrator allows the thrust vectoring control to be maintained near zero deflection or some other reference input.

The final two controller states are created by second-order dynamic compensation to provide additional regulation of the short period mode. This compensation is designed by heavily weighting the error between the two dynamic compensator state outputs and the open-loop short-period mode.[6,13] Results in both references show that the dynamic compensation increased robustness of the controller with respect to parameter variations, and the first reference shows increased short-period regulation during control element failures. The compensation has been incorporated in this application based on past robustness results. The second-order dynamic compensation is variable and included in the K_u gains [Eq. (24)]. Outputs from all six controller states augment the three plant outputs, giving a total of nine feedback variables used in the variable-gain design example. The sampling period used is 0.031 s to correspond with an existing real-time simulation.

There are several possible gain-scheduled parameters p that might be used for the variable feedback-gain matrix [Eq. (10)], but since this controller is for high-α research, a gain schedule that is proportional to α has been selected. The function used is

$$p = \frac{\alpha - \alpha_o}{\alpha_o} \tag{26}$$

where α_o is the reference value (5 deg) of the lowest α-trim case and is arbitrarily selected to make $p = 0$ for the first model. Values of p for the four models used in the design are 0, 2, 6, and 11. Each of the models have equal weighting in the global cost [Eq. (2)].

Linear Analysis

Design goals include the trading off of several typical frequency and time response control system criteria. Frequency domain goals include closed-loop eigenvalues with damping ratios (excluding actuator dynamics and the phugoid mode) of at least 0.5, bandwidth as high as possible with the constraint that gain attenuation must be at least 20 dB at 50 rad/s, gain margins of 6 dB, and phase margins of at least 40 deg. Time response goals include smooth responses with little or no overshoot, nonsaturating controls for large α changes (5–60 deg), and zero steady-state errors for the regulated variables. After performing the various analyses, penalty weights Q and R [Eq. (1)] and covariances W and V [Eqs. (7) and (8)] are modified for each operating condition to adjust the design. The procedure is iterative, similar to other LQ-type design techniques.

Table 2 gives the s plane, closed-loop eigenvalues, and damping ratios for the variable-gain design at the four design points. All closed-loop eigenvalues are computed in the z plane (discrete), but are shown in the s plane for simplicity using the inverse z transform [$s = \ell_n(z)/T$]. Each model corresponds to a flight condition as described in the previous section. The six most negative eigenvalues under model 1 correspond to actuator dynamics and the n_z filter. The closed-loop short-period eigenvalues are at $-3.19 \pm j1.91$ with a damping ratio of 0.86. The two eigenvalues nearest the origin represent the phugoid, which has a reduced frequency and is more heavily damped than the corresponding open-loop phugoid. The phugoid is not directly controlled and the fact that the closed-loop phugoid is changed from the open-loop phugoid is due to coupling through the feedback measurements. The closed-loop, short-period eigenvalues for models 2–4 are $-0.96 \pm j1.17$, $-0.79 \pm j0.84$, and $-0.72 \pm j1.04$, respectively. Comparing all four models, the smallest damping ratio

Table 2 Closed-loop eigenvalues

Model 1			Model 2		
Real	Imaginary	Damping	Real	Imaginary	Damping
−0.622E + 02	0.857E + 02	0.59	−0.621E + 02	0.852E + 02	0.59
−0.622E + 02	−0.857E + 02	0.59	−0.621E + 02	−0.852E + 02	0.59
−0.496E + 02	0.000E + 00	1.00	−0.511E + 02	0.000E + 00	1.00
−0.301E + 02	0.000E + 00	1.00	−0.306E + 02	0.000E + 00	1.00
−0.166E + 02	0.337E + 02	0.44	−0.223E + 02	0.000E + 00	1.00
−0.166E + 02	−0.337E + 02	0.44	−0.153E + 02	0.333E + 02	0.42
−0.158E + 02	0.000E + 00	1.00	−0.153E + 02	−0.333E + 02	0.42
−0.531E + 01	0.600E + 01	0.66	−0.693E + 01	0.000E + 00	1.00
−0.531E + 01	−0.600E + 01	0.66	−0.461E + 01	0.372E + 01	0.78
−0.319E + 01	0.191E + 01	0.86[a]	−0.461E + 01	−0.372E + 01	0.78
−0.319E + 01	−0.191E + 01	0.86[a]	−0.960E + 00	0.117E + 01	0.63[a]
−0.147E + 01	0.478E + 00	0.95	−0.960E + 00	−0.117E + 01	0.63[a]
−0.147E + 01	−0.478E + 00	0.95	−0.862E + 00	0.000E + 00	1.00
−0.155E + 00	0.000E + 00	1.00	−0.187E + 00	0.000E + 00	1.00
−0.100E − 01	0.739E − 02	0.80	−0.117E − 01	0.133E + 00	0.09
−0.100E − 01	−0.739E − 02	0.80	−0.117E − 01	−0.133E + 00	0.09
Model 3			Model 4		
Real	Imaginary	Damping	Real	Imaginary	Damping
−0.621E + 02	0.851E + 02	0.59	−0.621E + 02	0.849E + 02	0.59
−0.621E + 02	−0.851E + 02	0.59	−0.621E + 02	−0.849E + 02	0.59
−0.517E + 02	0.000E + 00	1.00	−0.507E + 02	0.000E + 00	1.00
−0.317E + 02	0.000E + 00	1.00	−0.329E + 02	0.000E + 00	1.00
−0.280E + 02	0.000E + 00	1.00	−0.285E + 02	0.000E + 00	1.00
−0.150E + 02	0.332E + 02	0.41	−0.148E + 02	0.333E + 02	0.41
−0.150E + 02	−0.332E + 02	0.41	−0.148E + 02	−0.333E + 02	0.41
−0.498E + 01	0.370E + 01	0.80	−0.886E + 01	0.106E + 01	0.99
−0.498E + 01	−0.370E + 01	0.80	−0.886E + 01	−0.106E + 01	0.99
−0.379E + 01	0.675E + 00	0.98	−0.221E + 01	0.195E + 01	0.75
−0.379E + 01	−0.675E + 00	0.98	−0.221E + 01	−0.195E + 01	0.75
−0.791E + 00	0.841E + 00	0.69[a]	−0.720E + 00	0.104E + 01	0.57[a]
−0.791E + 00	−0.841E + 00	0.69[a]	−0.720E + 00	−0.104E + 01	0.57[a]
−0.929E − 01	0.000E + 00	1.00	−0.317E + 00	0.000E + 00	1.00
−0.566E − 01	0.177E + 00	0.30	−0.204E + 00	0.432E − 01	0.98
−0.566E − 01	−0.177E + 00	0.30	−0.204E + 00	−0.432E − 01	0.98

[a]Short period.

(excluding the phugoid and actuators) is 0.57, which is the short-period mode for model 4. The open-loop damping ratio for the corresponding case is 0.004 (Table 1). All other damping ratios are greater than 0.63. The controller (not shown) is completely stable except for one eigenvalue at the origin due to the α or q integrator for each model.

Single-loop Bode analysis was done for all four models. Although not shown in this paper, the worst case gain and phase margin at the plant input is 13.5 dB and 46 deg for the thrust vectoring control loop of model 4. Figures 2 contain the structured singular value[14] for a multiplicative error when breaking the control loop for each model at the plant input (Fig. 2a) or the plant output (Fig. 2b). The numbers on the curves refer to the model. The curve for model 1 is always above 1.0 for the plant input, and only goes below 1.0 at the lower frequencies for the plant output; the minimum is at 0.01 rad/s, which is the closed-loop phugoid frequency. Model 2 results show minimum singular values slightly less than 0.9 (excluding the phugoid frequency, which is very lightly damped) at both the plant input and the plant output. The lowest singular value at the plant input is slightly greater than 0.6 for model 4, and the lowest singular value at the plant output is approximately 0.48 for models 3 and 4. These last data indicate that the maximum magnitude of uncertainty in each output loop must be less than 0.48 for stability. The stability margin δ_{sm} for a multiplicative error at the plant output is given as

$$\delta_{sm} = \frac{1}{\mu[(I-PG)^{-1}PG]} \tag{27}$$

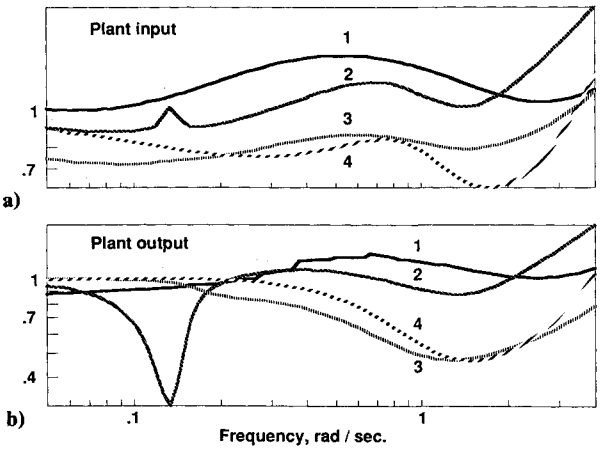

Fig. 2 Singular value, multiplicative error: a) plant input; b) plant output.

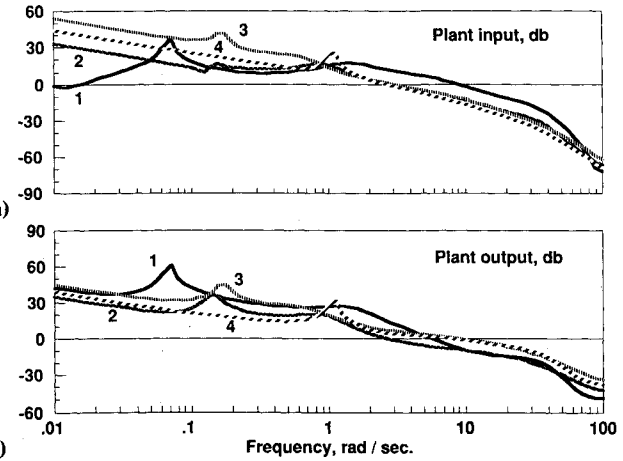

Fig. 3 Singular value, loop transfer: a) plant input, dB; b) plant output, dB.

where μ represents the structured singular value, P is the plant, and G is the controller. A similar form is used for the plant input. The minimum singular values can also be interpreted in terms of multivariable phase and gain margins. The phase margin at the plant input is 35 deg and the gain margin is 4.1 dB on the high side and -8 dB on the low side. Similarly, the plant output has a phase margin of 28 deg and a gain margin of 3.4 dB on the high side and -5.7 dB on the low side. The multivariable margins are conservative since they represent a simultaneous phase change or a simultaneous gain change in all channels.

The maximum singular value for the loop transfer is shown in Figs. 3. Figure 3a contains the singular values in decibels for all four models when the loop is broken at the plant input (GP), and Fig. 3b shows the singular values when the loop is broken at the plant output (PG). The lightly damped, open-loop phugoid frequency for models 1-3 are shown by the sharp peaks in the singular-value curves. The sharp peak in the curves for model 4 represent the open-loop short period, which has a damping ratio of 0.004, whereas the open-loop phugoid for model 4 is highly damped at 0.61. The plots show that the crossover frequency at the plant input is less than 9 rad/s for model 1 and less than 3 rad/s for the other three models. All models show attenuation by at least 33 dB at 50 rad/s for the plant input and by 21 dB at the plant output.

Nonlinear Simulation

A nonlinear six-degree-of-freedom, quasi-static-elastic dynamic model is used for batch simulations. The aerodynamic tables, generated from a wind-tunnel-derived data base, have an α range from -10 to 90 deg and a sideslip range of ± 20 deg. All control surfaces include constant position and rate limits. The nonlinear simulation has control laws for each of the longitudinal, lateral, and directional axes. Each of the control laws are consistent with and representative of the actual control laws, modified for thrust vectoring, for the high-performance airplane model in the real-time simulator at NASA Langley Research Center. The existing longitudinal controller is replaced by the variable-gain longitudinal controller described in this paper, whereas the lateral and directional controllers remain unchanged. An inertial coupling signal, normally included in the longitudinal controller to compensate for lateral-directional rotation rates, is not included in the simulations to be described. In the nonlinear simulation, variable-gain scheduling is used for all feedback gains, whereas linear interpolation is used for the feed-forward gains.

Practical Aspects

Three practical flight aspects that are not considered during the linear design phase are described. The first is the need to use multimode controllers and to smoothly change modes during flight. As discussed previously, two modes have been included in the variable-gain design with a transition between the modes.

The second practical aspect is to incorporate trim schedules in the nonlinear simulation. Linear designs are based on flap and thrust levels for a particular airplane trim case. In the batch simulation, flap and power-level angle schedules are incorporated as a function of α to make the simulation perform as close as possible to the desired trims. The schedules are shown in Figs. 4 as a function of α and include the leading- and trailing-edge left flaps, power-lever angle command (PLAC), and thrust. Units of Figs. 4a-c are degrees and Fig. 4d is in thousands of pounds. The PLAC schedule is based on the trim thrust (which is related to α) from the linear design and is incorporated to simulate the action of a pilot who would normally push the throttle forward for increased thrust as the airplane pitches up. During a time simulation, the thrust level lags PLAC by approximately 1 s.

A third practical aspect is a dead-band nonlinearity in the δ_v control. Figure 5 shows the effective turning angle as a func-

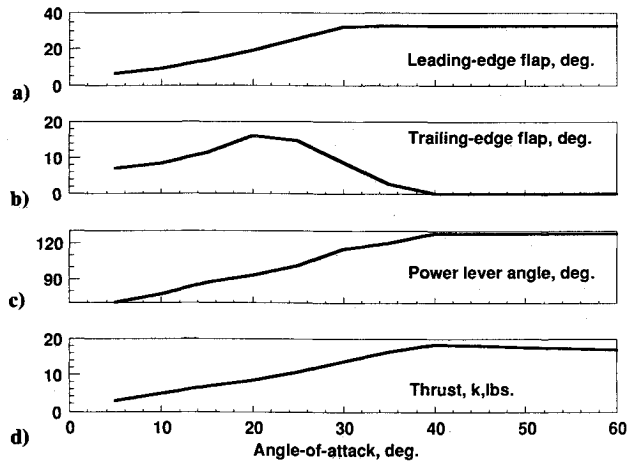

Fig. 4 Flap and thrust schedule: a) leading-edge flap, deg; b) trailing-edge flap, deg; c) power-level angle, deg; d) thrust, k, lb.

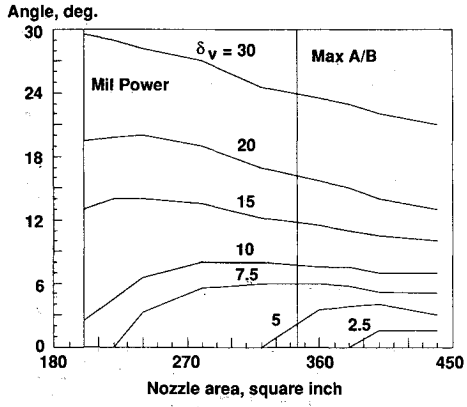

Fig. 5 Effective turning angle as a function of thrust vectoring deflection and nozzle area.

tion of thrust vectoring deflection and nozzle area at an altitude of 15,000 ft. As an example, for a nozzle area of 320 in.^{2} and a δ_v deflection of 5 deg, there is no effective turning angle. The normal dead bands at the high-alpha cases considered are approximately ± 6 deg out of a total range of ± 25 deg. The thrust vectoring dead band has an effect on the control derivatives that are used for the linear designs. For cases where δ_v is trimmed to zero deflection, the dead band must be accounted for in all perturbations from trim. The δ_v control derivatives used in the linear designs have been adjusted to compensate for this dead band. During nonlinear simulation, the effective thrust vectoring dead band is estimated as a function of nozzle area. This dead band is then added to the thrust vectoring command to get the total δ_v command.

Variable-Gain Results

Figures 6 and 7 illustrate the longitudinal variable-gain control for a pitch-up, pitch-down command y_m using the four design points described earlier in this paper. Initially, y_m represents a commanded q of 0 deg/s and then changes to 60 deg/s at 0.2 s. As α increases, the mode transitions to an α-command system and y_m represents 60 deg of α. At 8 s into the run, y_m commands α to increase to 35 deg, and at 16 s, y_m reverts back to the initial command mode of 0 deg/s for q.

The α curve starts at 5-deg trim and reaches 55 deg in less than 3.5 s, then slowly reaches the initial command of 60 deg. During this same time period, the pitch angle reaches 90 deg, with the flight path angle (not shown) peaking at 30 deg before dropping off and q reaches a peak of 40 deg/s. At 8 s, α starts to decrease to the commanded values of 35 deg, reaching this value within 3 s with a slight overshoot. The final command shows α decreasing to the initial trim value of 5 deg approximately 3 s after the command is initiated while the q curve settles out to 0 deg/s in steady state. Both controls $\delta_{s,l}$ and $\delta_{v,l}$, representing the left stabilator and left thrust vectoring surface positions, respectively, remain within the linear range. With the exception of the initial transient response, $\delta_{v,l}$ operates near the dead band. The p curve, representing the gain-scheduling parameter, has the shape of α [Eq. (26)]. The ERROR curve represents the difference between y_m and the regulated variable and is a function of the mode. Initially, ERROR is the

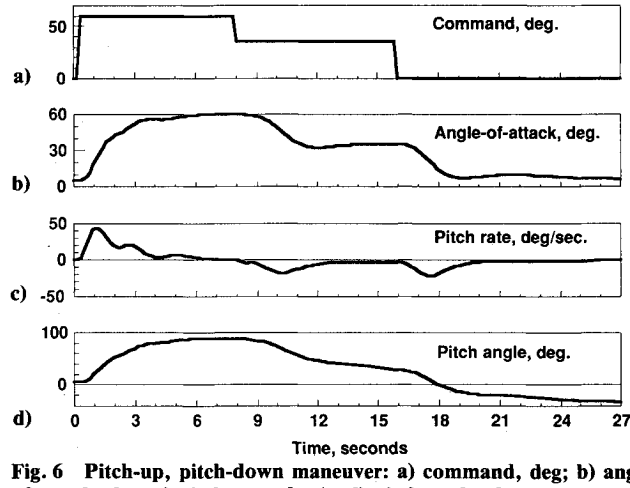

Fig. 6 Pitch-up, pitch-down maneuver: a) command, deg; b) angle of attack, deg; c) pitch rate, deg/s; d) pitch angle, deg.

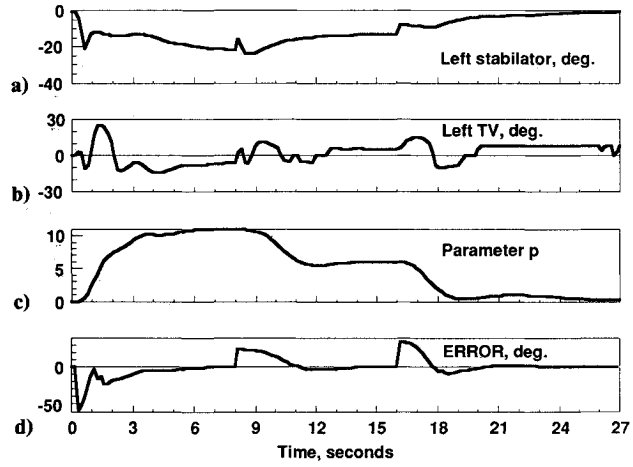

Fig. 7 Pitch-up, pitch-down maneuver: a) left stabilator, deg; b) left TV, deg; c) parameter p; d) ERROR, deg.

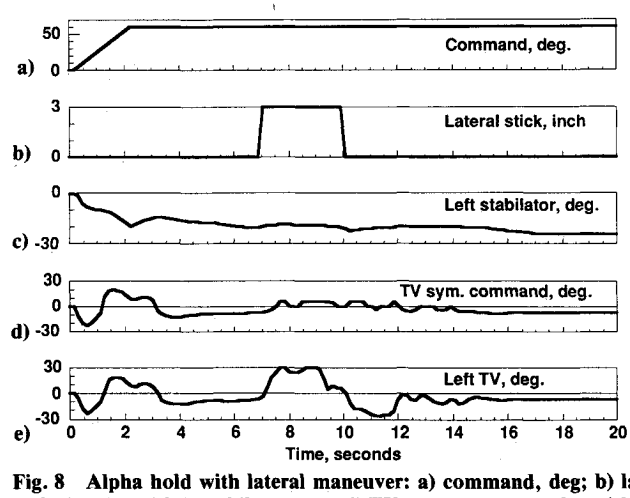

Fig. 8 Alpha hold with lateral maneuver: a) command, deg; b) lateral stick, in.; c) left stabilator, deg; d) TV sym. command, deg; e) left TV, deg.

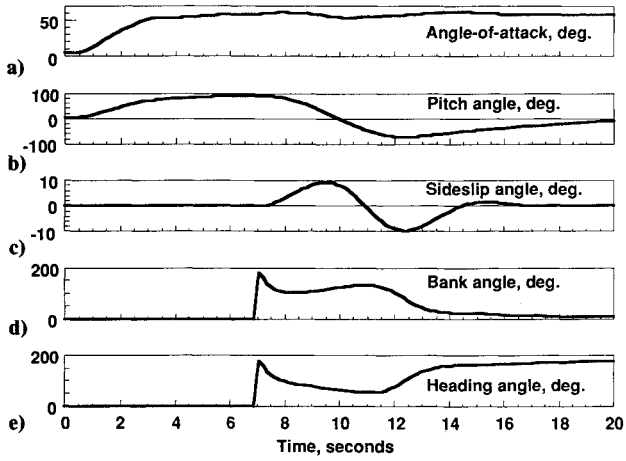

Fig. 9 Alpha hold with lateral maneuver: a) angle of attack, deg; b) pitch angle, deg; c) sideslip angle, deg; d) bank angle, deg; e) heading angle, deg.

difference between y_m and q. As α increases, ERROR becomes the difference between y_m and α. Finally, during the last 8 s of the simulation, ERROR is again the difference between y_m and q. Notice that ERROR goes to zero during all three steady-state periods.

The final set of plots, Figs. 8 and 9, illustrate the ability of the variable-gain design to hold α while performing a Herbst-like maneuver.[15] The longitudinal control shows y_m ramping from 0 deg/s to 60 deg in 2 s. Seven seconds into the run, when α is 60 deg and pitch angle slightly greater than 90 deg, a full lateral stick (PCA) is applied. The lateral command is maintained for 3 s as the airplane rolls about the velocity vector, illustrated by changes in Euler angles. At 11 s, PCA is returned to zero. At this time, there is a slight decrease in α, which then returns to the commanded value. After the rolling motion stops, the airplane nose pulls through negative θ and then heads to nose level. At the end of this maneuver, the airplane is heading in the opposite direction, almost wings level, while holding α at 60 deg and with a slight nose down, resulting in a flight-path angle of -70 deg.

One important feature of the control approach can be observed from the curves $\delta_{v,c}$ (thrust vectoring symmetric command) and $\delta_{v,l}$. In the simulation, the longitudinal and lateral-directional thrust vectoring commands are summed prior to driving the control surfaces, with the longitudinal signal having priority. Excluding the initial transient while α is increasing, $\delta_{v,c}$ remains close to the dead-band limits because of the integrator on the longitudinal thrust vectoring control command. During the lateral maneuver, full thrust vectoring moments are applied by the lateral-directional controller to maximize roll rate because $\delta_{v,c}$ is maintained near zero deflection angle. A second benefit of maintaining $\delta_{v,c}$ near zero deflection angle is to reduce heating on the vanes by keeping them at the edge of the exhaust plume.

Conclusions

A relatively new optimal variable-gain output feedback control design methodology is applied to an aircraft operating over a highly nonlinear flight regime that includes high angle-of-attack α flight. The advantage of using an output feedback design algorithm is that relatively high-order dynamic models can be included for more accurate dynamic representation without the necessity of feeding back all states. The dynamics may thus include actuator and sensor dynamics in addition to the short-period and phugoid modes. The control law demonstrates the applicability of an integrated design approach in which a design for two flight control modes and four flight conditions are simultaneously considered. The two flight modes are an angle-of-attack command mode at high α and a pitch-rate command mode at low α with a transition between the two modes, and the four flight conditions are for α of 5, 15, 35, and 60 deg at constant altitude. In this initial application, the feedback gain matrix varies as a function of one gain schedule parameter α. Results from the four design models show the following: 1) the damping ratio of the closed-loop eigenvalues meet design goals with the lowest damping ratio being for the model at $\alpha = 60$ deg; 2) the single-loop gain and phase margins meet design goals, whereas the more conservative multiloop analysis shows margins that are less than desired; 3) the gain attenuation meets the high-frequency objective with reasonable crossover frequencies; 4) the nonlinear time response for large angular maneuvers over the α range do not saturate the controls; 5) the response for large pitch-up and pitch-down maneuvers takes approximately the same time; and 6) the α regulation is maintained within -5 deg from the nominal angle during a high-α lateral maneuver.

References

[1]Halyo, N., and Broussard, J. R., "Investigation, Development, and Application of Optimal Output Feedback Theory—Volume I: A Convergent Algorithm for the Stochastic Infinite-Time Discrete Optimal Output Feedback Problem," NASA CR-3828, Aug. 1984.

[2]Halyo, N., Moerder, D. D., Broussard, J. R., and Taylor, D. B., "A Variable-Gain Output Feedback Control Design Methodology," NASA Contract NAS1-17493, NASA CR-4226, March 1989.

[3]Halyo, N., "A Variable-Gain Output Feedback Control Design Approach," *Proceedings of the AIAA Guidance, Navigation, and Control Conference,* AIAA, Washington, DC, Aug. 1989.

[4]Moerder, D. D., Halyo, N., Broussard, J. R., and Caglayan, A. K., "Application of Precomputed Control Laws in a Reconfigurable Aircraft Flight Control System," *Journal of Guidance, Control, and Dynamics,* Vol. 12, No. 3, 1989, pp. 325-333.

[5]Ostroff, A. J., and Hueschen, R. M., "Reconfigurable Multivariable Control Law for Commercial Airplane Using a Direct Digital Output Feedback Design," NASA TM-85759, Feb. 1984.

[6]Ostroff, A. J., and Hueschen, R. M., "Investigation of Control Law Reconfigurations to Accommodate a Control Element Failure on a Commercial Airplane," *Proceedings of the 1984 American Control Conference,* American Automatic Control Council, Piscataway, NJ, June 1984.

[7]Ostroff, A. J., "Techniques for Accommodating Control Effector Failures on a Mildly Statically Unstable Airplane," *Proceedings of the 1985 American Control Conference,* American Automatic Control Council, Piscataway, NJ, 1985.

[8]Broussard, J. R., "Design, Implementation and Flight Testing of PIF Autopilots for General Aviation Aircraft," NASA Contract NAS1-16303, NASA CR-3709, July 1983.

[9]Halmos, P. R., *Finite-Dimensional Vector Spaces,* Springer-Verlag, New York, 1974, p. 98.

[10]Maybeck, P. S., *Stochastic Models, Estimation, and Control,* Vol. 3, Academic, New York, 1982.

[11]Broussard, J. R., and O'Brien, M. J., "Feedforward Control to Track the Output of a Forced Model," *IEEE Transactions on Automatic Control,* Vol. AC-25, No. 4, 1980, pp. 851-854.

[12]Klein, V., Ratvasky, T. P., and Cobleigh, B. R., "Aerodynamic Parameters of High-Angle-of-Attack Research Vehicle (HARV) Estimated from Flight Data," NASA TM 102692, Aug. 1990.

[13]Broussard, J. R., and Halyo, N., "Active Flutter Suppression Using Optimal Output Feedback Digital Controllers," NASA Contract NAS1-16772, NASA CR-165939, May 1982.

[14]Doyle, J., "Analysis of Feedback Systems with Structured Uncertainties," *IEEE Proceedings,* Vol. 129, Pt. D., No. 6, 1982, pp. 242-250.

[15]Herbst, W. B., "Future Fighter Technologies," *Journal of Aircraft,* Vol. 17, No. 8, 1980, pp. 561-566.